Upward Vertical Two-Phase Flow Through an Annulus—Part I: Single-Phase Friction Factor, Taylor Bubble Rise Velocity, and Flow Pattern Prediction

E. F. Caetano[1]

O. Shoham

J. P. Brill

The University of Tulsa,
Tulsa, OK 74104

Upward gas-liquid flow through vertical concentric and fully eccentric annuli was studied both experimentally and theoretically. A flow system was designed and constructed for this study. The system consists of a 16-m long vertical annulus with 76.2-mm i.d. casing and 42.2-mm o.d. tubing. A comprehensive experimental investigation was conducted for both concentric and fully eccentric annuli configurations, using air-water and air-kerosene mixtures as the flowing fluids. Included were definition and classification of the existing flow patterns and development of flow pattern maps. Measurements of volumetric average liquid holdup and average total pressure gradient were made for each flow pattern for a wide range of flow conditions. Additional data include single-phase friction factor values and Taylor bubble rise velocities in a stagnant liquid column. Data analysis revealed that application of the hydraulic diameter concept for annuli configurations is not always adequate, especially at low Reynolds number flow conditions. A more rigorous approach was thus required for accurate prediction of the flow behavior, especially for two-phase flow. Part I of the study includes experimental data and analyses of single-phase friction factor, Taylor bubble rise velocity, and flow pattern transition boundaries.

Introduction

An annulus is characterized by the existence of two circular pipes, where the flow occurs through the area bounded by the outer pipe inner wall and the inner pipe outer wall. Two geometrical parameters identify these configurations: the annulus pipe diameter ratio, and the degree of eccentricity. The annulus pipe diameter ratio accounts, to some extent, for the flow area and is expressed by

$$K=\frac{D_T}{D_C} \tag{1}$$

where D_T is the outer diameter of the inner pipe (tubing) and D_C is the inner diameter of the outer pipe (casing). The degree of eccentricity accounts for the displacement of the inner pipe center from the outer pipe center and is expressed by

$$e=\frac{2\ \mathrm{DBC}}{(D_C-D_T)} \tag{2}$$

where DBC is the distance between the pipe centers. Annuli can have eccentricity values varying from zero to one. Figure 1 shows cross sections of annuli with the same pipe diameter ratio value, K, and for eccentricities of 0.0, 0.5, and 1.0.

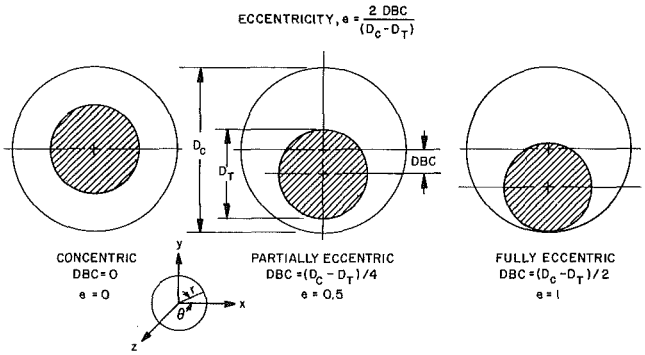

Fig. 1 Annuli configuration

In the petroleum industry, flow in wells normally occurs in a tubing string. However, many oil wells with high production rates produce through the casing-tubing annulus. This trend is dictated by economics, multiple completions and regulated production rates. Although few in number when compared with all producing wells, these "casing flow" wells account for a significant part of the world oil production.

[1]Presently with Petrobras, Rio de Janeiro, Brazil.

Contributed by the Petroleum Division for publication in the JOURNAL OF ENERGY RESOURCES TECHNOLOGY. Manuscript received by the Petroleum Division, September 15, 1990; revised manuscript received June 23, 1991.

Other applications of casing flow are found in wells under various types of artificial lift. In sucker rod pumping wells, a rod string is installed inside the tubing string to connect the prime mover unit on the surface to the pump at the bottom of the well. The fluids are pumped upward through the tubing-rod string annulus. Casing flow can also occur in gas well production. In order to remove or "unload" undesirable liquids that can accumulate at the bottom of these wells, a siphon tube is often installed inside the tubing string. The normal permanency of the siphon tube in the tubing string requires the fluids to flow upward through the tubing string-siphon tube annulus.

Annuli have been treated in the past based on the hydraulic diameter concept. The hydraulic diameter is four times the area for flow divided by the wetted perimeter. For annulus configurations

$$D_H = D_C - D_T \tag{3}$$

However, the hydraulic diameter is not always the most representative characteristic dimension for flow in an annulus. A clear understanding of flow in an annulus must be achieved in order to determine appropriate characteristic dimensions.

The objective of this study is to investigate, experimentally and theoretically, upward gas-liquid two-phase flow in vertical concentric and fully eccentric annuli. The experimental part includes flow pattern definitions, determination of the transition boundaries, development of flow pattern maps, and measurements of the average volumetric liquid holdup and average pressure gradient for each existing flow pattern. The theoretical part includes development of a flow pattern prediction model, and construction of models for each flow pattern to predict average volumetric liquid holdup and pressure drop. These models can be integrated into an overall computer simulator for field design applications.

Part I of the study includes experimental data and analyses of single-phase friction factor, Taylor bubble rise velocity, and flow pattern transition boundaries in annuli configurations.

Literature Review

An inspection of the literature shows that only a few studies have been conducted on flow through an annulus. Following is a literature review on some pertinent aspects of single phase and two phase flow through an annulus. These include single-phase flow friction factors, Taylor bubble rise velocity, and two-phase flow pattern transition boundaries.

Friction Factor in a Single-Phase Flow. For noncircular conduits, single-phase flow friction factors are often determined through the application of the hydraulic diameter concept. However, this concept is better suited for high degrees of turbulence. Predictions of friction factors for annuli have been presented in several studies as a function of the existing flow regime.

For laminar flow, a rigorous treatment of the flow field is possible for any annulus configuration. Analytical solutions for both the velocity profile and friction factor for a concentric annulus are given by Bird et al. (1976). Combining the developments by Snyder and Goldstein (1965) and Tosun (1984), analytical solutions can also be found for these flow parameters for an eccentric annulus. These solutions are presented in a later section.

In turbulent flow, even for circular pipes, the mechanisms of turbulence are by no means fully understood. However, various semi-empirical and analytical models have successfully been employed for predicting the velocity distribution and pressure gradient. In noncircular configurations, where the transport phenomena are intrinsically more complex than for circular pipes, the formulation of an analytical model is even more complicated. The literature survey identified three ways to predict the flow behavior of a turbulent flow field in an annulus: empirical correlations, semi-empirical correlations, and application of universal velocity distributions.

Empirical correlations involve application of curve-fitting techniques to experimental data to predict an overall flow quantity such as friction factor. The resulting friction factor correlations normally take the form of the Blasius-type expression

$$f = C\mathrm{Re}^{-x} \tag{4}$$

where Re is the Reynolds number, and the coefficients C and x are determined empirically. Examples include the correlations of Davis, Knudsen and Katz, Carpenter et al. (Knudsen and Katz, 1954) and Dodge (1964). Winkler (1968) successfully used the Dodge correlation for flow in an annulus; however, he noted that this procedure did not take into account the annulus pipe diameter ratio.

Semi-empirical approaches involve using experimental data for turbulent flow in combination with characteristics of laminar flow in the same noncircular configuration. An example of this prediction category is the procedure of Gunn and Darling (1963). An important conclusion by Gunn and Darling is that the similarity existing between friction factors for circular and noncircular configurations in the laminar region is also accompanied by a similarity in the turbulent region. Using dimensional analysis, they showed that for turbulent flow in noncircular sections, the following functional dependency for friction factor exists.

Nomenclature

A = area
C = constant
C_1 = dimensionless bubble rise velocity parameter
D = diameter
DBC = distance between centers of pipes in annulus
e = annulus eccentricity
E = bubble eccentricity
f = Fanning friction factor
F = friction geometry parameter
g = acceleration of gravity
H = in-situ volume fraction
K = annulus pipe diameter ratio
L = characteristic dimension, length
M = bubble aspect ratio
N_{Ar} = dimensionless Archimedes no.
$N_{\mathrm{Eö}}$ = dimensionless Eötvos no.
N_μ = dimensionless inverse viscosity no.
p = pressure
Re = dimensionless Reynolds no.
V = local or in-situ velocity
x = exponent in Blasius equation
z = elevation
η = ordinate in complex plane
μ = dynamic viscosity
π = static pressure and gravitation combined effects ($\pi = p - \rho g z$)
ρ = density
σ = surface tension
ϕ = function
$< >$ = average over cross section

Subscripts

C = casing, circular
CA = concentric annulus
EA = eccentric annulus
EP = equi-periphery
G = gas
H = hydraulic
i = inner
L = liquid, axial location
M = mixture
NC = noncircular
o = axial location, outer
P = pipe
SG = superficial gas
SL = superficial liquid
T = tubing
TB = Taylor bubble
z = axial
$0,\infty$ = free rise of discreet bubble

$$f_{NC} = \phi\left(\text{Re}, \frac{F_C}{F_{NC}}\right) \tag{5}$$

where Re is the Reynolds number and F_C and F_{NC} are the so-called friction geometry parameters for the circular and noncircular configurations, respectively. At low Reynolds numbers the friction factor is inversely proportional to the ratio F_C/F_{NC}. However, at high Reynolds numbers the friction factor becomes independent of the F_C/F_{NC} ratio. At intermediate values of Reynolds numbers the function given in Eq. (5) is established from suitable experimental data involving many noncircular types of configurations.

The third method of predicting friction factor values is the use of the velocity flow field. In general, the velocity flow field is not angular dependent in a concentric annulus, whereas, it is angular dependent in an eccentric annulus. The velocity field occurring under single-phase turbulent flow is generally presented in three different forms: contour maps (Dodge, 1964; Deissler and Taylor, 1955; Rothfus et al., 1966; Jonsson and Sparrow, 1966; Lawn and Elliott, 1972); law-of-the-wall (Deissler and Taylor, 1955; Rothfus et al., 1966; Jonsson and Sparrow, 1966; Lawn and Elliott, 1972; Quarmby, 1967; Rothfus and Newby, 1970; Rothfus et al., 1958); and, defect-law (Hinze, 1959). No further discussion is presented on this method as it has no bearing on the present study.

Taylor Bubble Rise Velocity. One of the most common flow patterns encountered in two-phase flow is slug flow. In this flow pattern the gas phase is concentrated in a large bullet-shaped bubble, termed a Taylor bubble. In order to adequately predict slug flow behavior, it is necessary to predict the rise velocity of these bubbles in stagnant liquid columns.

The terminal velocity with which a single bubble rises through a stagnant liquid column is governed by the interaction between buoyancy and the other forces acting on the bubble as a result of its shape and motion. For a negligible bubble viscosity these forces are liquid inertia, liquid viscous drag, and bubble gas-liquid surface tension. The equilibrium obtained between buoyancy and these forces is normally expressed in terms of the following dimensionless groups: Eötvos number, inverse viscosity number, and the Archimedes number, defined, respectively, by

$$N_{\text{Eö}} = \frac{gL^2(\rho_L - \rho_G)}{\sigma} \tag{6}$$

$$N_{\mu} = \frac{[gL^3(\rho_L - \rho_G)\rho_L]^{1/2}}{\mu_L} \tag{7}$$

$$N_{\text{Ar}} = \frac{\rho_L \sigma^{3/2}}{[\mu_L^4 g(\rho_L - \rho_G)]^{1/2}} \tag{8}$$

A general solution for a particular system involves a combination of all three dimensionless groups or, in a limiting case, only one of them. Wallis (1969) investigated the importance of each group in a given system and concluded that inertia is the dominant effect when

$$N_{\text{Eö}} > 100 \text{ and } N_{\mu} > 300$$

Viscosity is the dominant effect when

$$N_{\text{Eö}} > 100 \text{ and } N_{\mu} < 2$$

Finally, he determined that surface tension is the dominant effect in round, vertical tubes when

$$N_{\text{Eö}} = 3.37 \text{ and } N_{\mu}^2 = 6.2\, N_{\text{Ar}}$$

The fluid systems and conduit configurations used in the oil and gas industry and in many other cases are dominated by inertial effects. Based on the studies of Dumitrescu (Govier and Aziz, 1977) and Davis and Taylor (1950), the following expression is accepted for inertia dominated systems with negligible bubble density fluid in pipe flow:

$$V_{TB} = C_1\sqrt{gL} \tag{9}$$

where C_1, the dimensionless bubble rise velocity (Froude number), is 0.345, and the characteristic dimension is the pipe diameter D.

Taylor bubble rise velocity in noncircular pipes was studied by Griffith (1964), Sadotomi et al. (1982) and Grace and Harrison (1967). Griffith suggested the use of the diameter of the outer conduit, often called the "large" or "shroud" dimension, as the characteristic dimension. For a concentric annulus, the dimensionless bubble rise velocity parameter, C_1, was determined experimentally as a function of the annulus pipe diameter ratio, K. The bubble velocity was found to rise at a faster velocity as the pipe diameter ratio increases, for a constant outer pipe inner diameter. Hence, application of the hydraulic diameter concept as the characteristic dimension can result in a substantial error. The experiments also showed that the parameter C_1 reduces to the values expected in circular pipes and parallel plates as the pipe diameter ratio changes from zero to one, respectively.

Sadatomi et al. (1982) investigated the bubble rise phenomenon in circular, rectangular, triangular and concentric annuli. They recommended the use of an equi-periphery diameter, D_{EP} as the characteristic dimension, yielding the following expression for the rise velocity:

$$V_{TB} = 0.345\sqrt{gD_{EP}} \tag{10}$$

where

$$D_{EP} = D_C + D_T \tag{11}$$

Taylor bubble rise velocities in configurations with and without insertions were studied by Grace and Harrison (1967). Their basic experimental configuration was a vertical duct with a rectangular cross-sectional area. The insertions consisted of single or multiple rods, flat plates and rectangular cross section area ducts. They found that a bubble changes its shape from a circular-cap to an elliptical-cap and, in the limit, to a parabolic-cap shape. These new shapes are a function of the particular surface inserted, and provide faster rising velocities as compared to flow without insertions.

Flow Pattern Transition Boundaries. The literature reveals that very few studies have been carried out on flow pattern transitions in annuli configurations. Various aspects of two-phase flow in noncircular configurations were carried out by Sadatomi et al. (1982) and Salcudean et al. (Salcudean et al., 1983; Salcudean et al., 1983; Salcudean et al., 1983). The Sadatomi et al. investigation did not cover all possible flow patterns, and the Salcudean et al. studies were strictly for horizontal conditions. No other work on annuli flow is available at the present time.

Experimental Program

A test facility has been designed and constructed for this study. The facility is composed of two main parts: a vertical test section and a fluid handling system. The fluid handling system is a modification of the facility used by Mukherjee (1979). The vertical test section consists of a casing-tubing annulus to simulate casing flow. It is attached to a superstructure, track and lift device, which permits flow at any inclination angle.

Vertical Test Section. A schematic diagram of the vertical casing flow test section is given in Fig. 2. This part of the experimental facility is composed primarily of a transparent casing-tubing pipe arrangement (right), a by-pass pipe (left), a bottom set of actuated ball valves, a top set of actuated ball valves, a two-phase mixing tee (bottom); and a downcomer line (top-bottom).

The outer (casing) pipe is made of 88.9 mm o.d., 76.2 mm i.d. cast acrylic. The inner (tubing) pipe is made of 31.8 mm

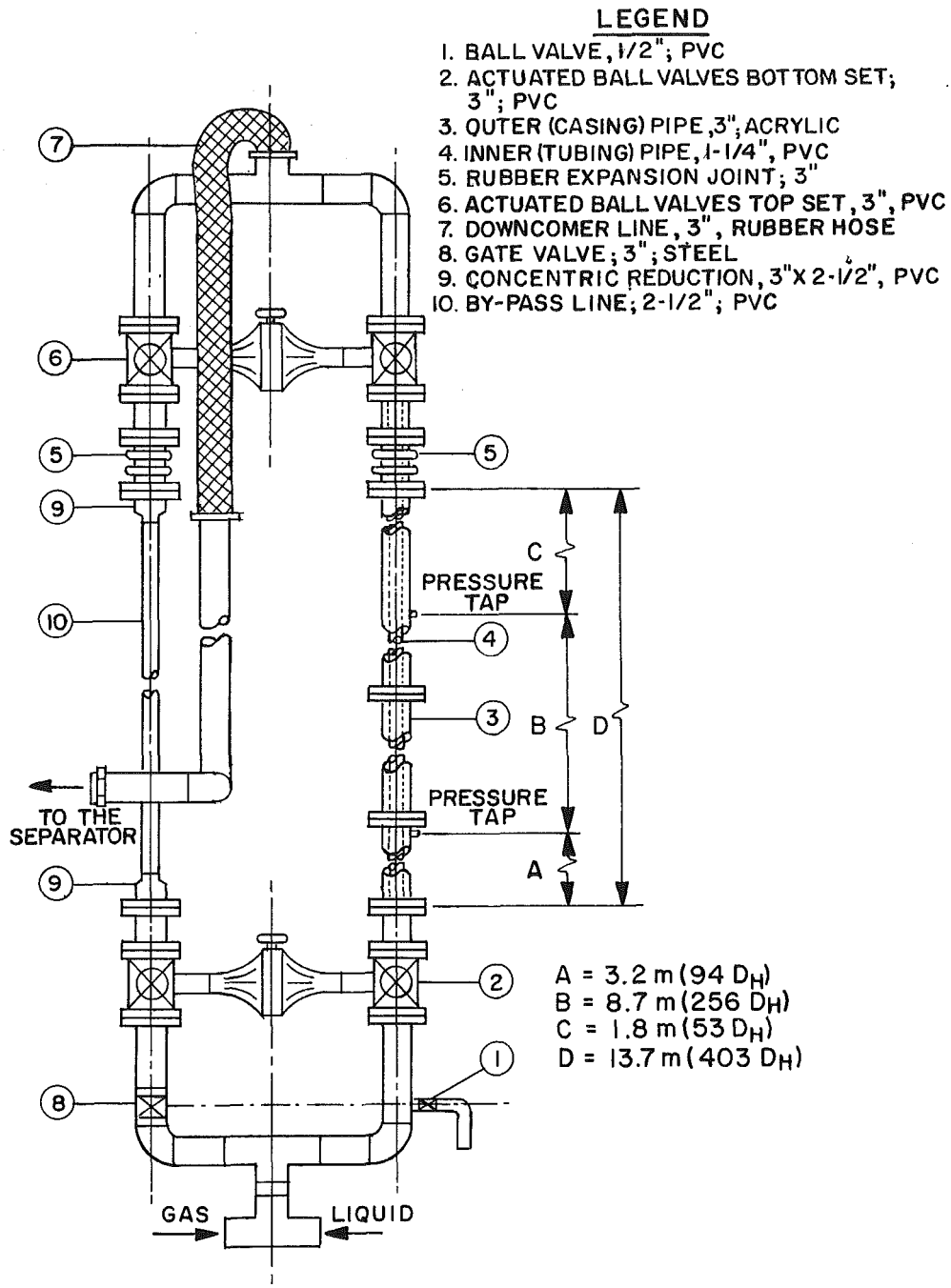

Fig. 2 Schematic diagram of test section

nominal diameter, 42.2 mm o.d. gray PVC. The annulus can be maintained concentric through the use of special inner pipe centralizer connectors consisting of four PVC pins, 3.2 mm o.d., 90 deg apart. Also, a fully eccentric casing-tubing annulus can be formed using 0.8 mm thick steel collar brackets around the inner pipe, at each cast acrylic flange, to attach the tubing to the casing wall.

Two pressure taps are installed in the transparent casing-tubing test section. The total length between these two taps is 8.7 m. The lower pressure tap is 3.5 m downstream of the lower ball valve face and the upper pressure tap is 2.3 m upstream from the upper ball valve face. In order to accommodate thermal expansions and contractions, rubber expansion joints were installed in the test section as shown in the figure.

The by-pass pipe is made of PVC, 63.5 mm nominal diameter and has approximately the same equivalent diameter as the casing-tubing annulus. The downcomer line is 76.2 mm nominal diameter PVC pipe. Two-phase flow into the downcomer line comes from either the transparent test section or the by-pass pipe. The bottom of the downcomer line connects to the return line and into a horizontal separator.

Each ball valve set has two ball valves with their stems coupled to a single-shaft of the actuator. The valves on the transparent test section side are normally open. A single electrical signal is a trigger for both actuators changing the conditions of the four valves with a constant time lag around 0.5 s.

Fluid Handling System. A schematic diagram of the fluid handling system is given in Fig. 3. The liquid phase is stored in two separate 9.54 m^3 storage tanks, one for water and one for kerosene. Either selected liquid is pumped by a separate centrifugal pump, with a maximum flow rate of 40.9 m^3/hr at 0.86 MPa. The liquid measurement manifold consists of

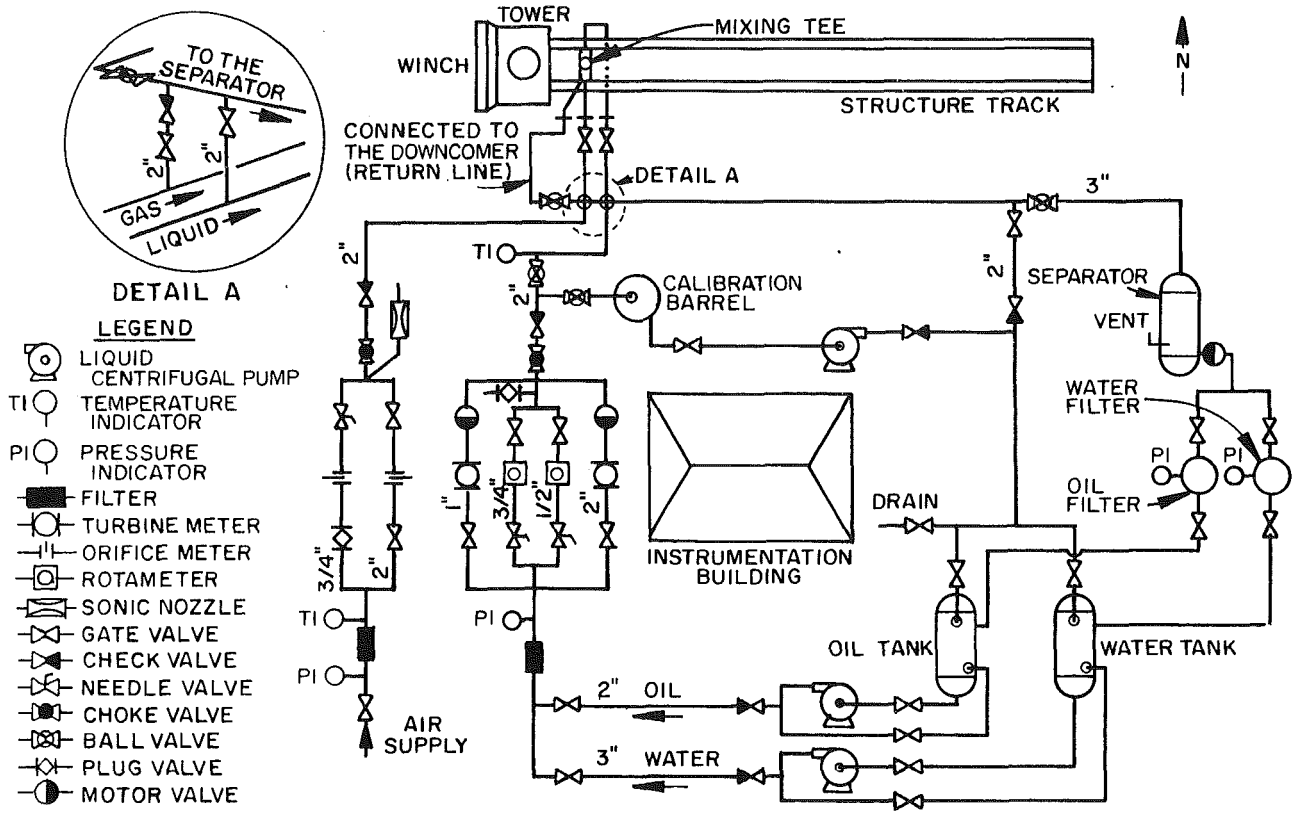

Fig. 3 Schematic diagram of fluid handling system

two turbine meters and two tapered rotameters. The flow rates are controlled by a choke valve downstream of the turbines, or needle valves upstream of the rotameters. Calibration of the liquid measurement devices is performed by using a calibrated tank and stopwatch technique.

Air supply is obtained from a compressor with a maximum output capacity of 1875 Nm^3/D at 0.83 MPa discharge pressure. A pressure controller is used to maintain a constant static pressure of 0.76 MPa upstream of the gas supply line. The gas measurement manifold consists of two orifice meters. The gas flow rate is controlled by a choke valve downstream of the orifice meters, and recorded by a Barton recorder and a 254-mm H_2O inclined manometer. The gas measurement devices were calibrated by using a sonic nozzle flow prover.

Single-Phase Flow Friction Factor Measurement. Turbulent single-phase flow friction factor values were experimentally determined for the concentric and fully eccentric annuli. This determination was made by measuring the friction pressure drop component between the two pressure taps. In single phase flow tests, the two taps are hydraulically connected to a Validyne Model DP15 variable reluctance differential pressure transducer. Due to the physical arrangement, this transducer measures the frictional pressure drop component only. The pressure transducer signal is sent to a demodulator and recorded on a strip chart recorder.

Taylor Bubble Rise Velocity Measurement. The Taylor bubble rise velocities were determined for bubbles with numerous different lengths, in both concentric and fully eccentric annuli for air-water and air-kerosene. Initially a stagnant liquid column is trapped between the ball valves of the transparent casing flow test section. A desired amount of liquid is drained through a manual valve upstream of the lower ball valve (see Fig. 2) to create a bubble. Once the drainage is complete, the ball valves are opened. After the bubble crosses the lower valve, both valves are closed again. The rising bubble length is determined by comparing it to a length scale located on the outside casing wall. The total rising time is measured by a stop watch. After this, the column is re-established and the process is repeated for the same or different bubble sizes.

Liquid Holdup Measurement. Two-phase flow liquid holdup was measured by the quick-closing ball valves technique. The total volume in the transparent vertical test section between the lower and upper ball valve sets is divided and scaled by unit percent marks of this total volume. These marks were placed on the outside wall of the casing pipe. Once steady-state conditions were established for a given test, a single electrical signal triggered the pneumatic actuator which closed the ball valves in the transparent test section and diverted the flow to the by-pass pipe by opening the ball valves on that side. On the transparent side, gravity separation of the phases occurred, and the average volumetric liquid holdup was read from the marks on the casing pipe wall. Each unit percent in volume corresponds to approximately 14.5 cm of length. Excellent repeatability was obtained in the liquid holdup measurements.

Pressure Drop Measurement. Two-phase flow pressure drop was measured at the two pressure taps in the vertical test section as shown in Fig. 2. Pressure measurements were made possible by using gas-liquid separator vessels ("splash pots") at each pressure tap in the test section. The vessels are made from acrylic cylinders, 1.22 m in length and 102 mm in diameter. Electric solenoid valves were installed at the single inlet and two outlets of each vessel. During each test run, the inlet and upper outlet of each separator were open. The gas and liquid phases flowed into the separator until equilibrium in pressure between the separator and the test section was reached. The pressure of the dry gas existing at the upper part of the separator was transmitted through a plastic tubing to the pressure measurement panel in the instrumentation building. After each measurement, the separator inlet was closed and the vessel drained through its solenoid valve at the bottom. The existing pressure difference was determined in the pressure panel by selecting one of three available Validyne Model DP15

variable reluctance differential pressure transducers, and recorded on a strip chart recorder. Calibration of the pressure transducers was accomplished by using U-tube manometers.

Single-Phase Friction Factor

As pointed out earlier, it is common practice to predict frictional pressure drop in noncircular conduits by applying the hydraulic diameter concept. However, this procedure should be limited to high Reynolds numbers, since unacceptable errors may occur for lower degrees of turbulence. Thus, more rigorous prediction methods are needed to predict friction losses in annuli under low or moderate degrees of turbulence.

Following is a brief summary of rigorous friction loss predictions in laminar flow, followed by an extension to turbulent flow in annuli. The solutions are compared to pipe flow predictions in order to show the errors which might result in applying the hydraulic diameter concept.

Laminar Flow. Friction factor in laminar flow is determined from solution of the continuity equation, equation of motion and Fanning equation. The solution is obtained for Newtonian, fully developed, steady-state, axial flow.

The Fanning equation can be written as

$$\pi_o - \pi_L = 2f\frac{L}{D_H}\rho < V_z >^2 \tag{12}$$

and the Reynolds number is given by

$$\mathrm{Re} = \frac{\rho < V_z > D_H}{\mu} \tag{13}$$

The Fanning friction factor in circular pipe, f_P, is given by

$$f_P = \frac{F_P}{\mathrm{Re}} = \frac{16}{\mathrm{Re}} \tag{14}$$

where F_P is a friction geometry parameter, having a constant value of 16 for pipe flow.

For a concentric annulus (Bird, 1976)

$$f_{CA} = \frac{F_{CA}}{\mathrm{Re}} = \frac{16}{\mathrm{Re}} \frac{(1-K)^2}{\left[\dfrac{1-K^4}{1-K^2} - \dfrac{1-K^2}{\ln(1/K)}\right]} \tag{15}$$

Thus,

$$F_{CA} = F_{CA}(K) = \frac{16(1-K)^2}{\left[\dfrac{1-K^4}{1-K^2} - \dfrac{1-K^2}{\ln(1/K)}\right]} \tag{16}$$

where f_{CA} is the Fanning friction factor and F_{CA} is the friction geometry parameter for a concentric annulus.

An analytical solution for laminar flow in an eccentric annulus, by using bipolar coordinate system was presented by Snyder and Goldstein (1965). Their solution was based on previous developments made by El-Saden (1961). The same technique was used by Redberger and Charles (1962), who presented a numerical solution for the problem. In a more recent work, Tosun (1984) developed an expression for the axial velocity in the x,y plane. Using the Fanning equation, the friction geometry parameter for an eccentric annulus is

$$f_{EA} = \frac{F_{EA}}{\mathrm{Re}} = \frac{1}{\mathrm{Re}} \frac{4(1-K)^2(1-K^2)}{\phi \sinh^4 \eta_o} \tag{17}$$

and

$$F_{EA} = F_{EA}(K,e) = \frac{4(1-K)^2(1-K^2)}{\phi \sinh^4 \eta_o} \tag{18}$$

where

$$\cosh \eta_i = \frac{K(1+e^2)+(1-e^2)}{2Ke} \tag{19}$$

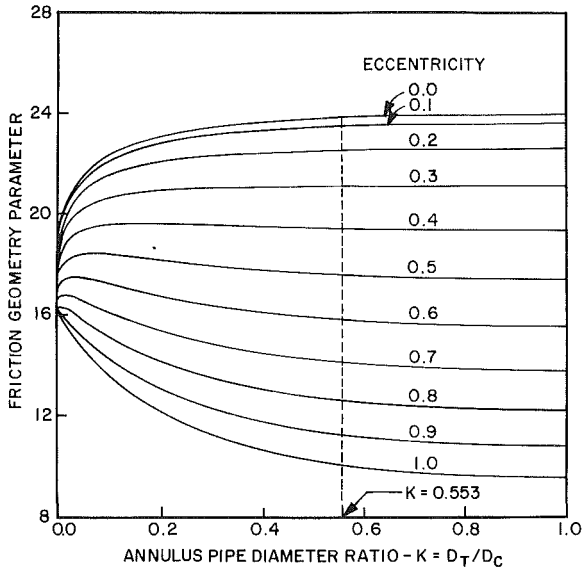

Fig. 4 Friction geometry parameter in annuli and circular pipes (laminar single-phase flow at same Reynolds number)

$$\cosh \eta_o = \frac{K(1-e^2)+(1+e^2)}{2e} \tag{20}$$

and

$$\phi = (\coth \eta_i - \coth \eta_o)^2 \left[\frac{1}{\eta_o - \eta_i} - 2\sum_{n=1}^{\infty} \frac{2n}{\exp^{(2n\eta_i)} - \exp^{(2n\eta_o)}}\right] + \frac{1}{4}\left(\frac{1}{\sinh^4 \eta_o} - \frac{1}{\sinh^4 \eta_i}\right) \tag{21}$$

Although an infinite series term is involved, the number of terms can be truncated after several terms. As before, f_{EA} is the Fanning friction factor and F_{EA} is the friction geometry parameter for an eccentric annulus.

Friction Factor Behavior Comparison. The solutions obtained for the friction factors in circular pipe, concentric annulus and eccentric annulus under laminar flow can be used to evaluate and compare friction loss behavior in these different configurations. Assuming that all configurations have the same hydraulic diameter and Reynolds number, comparison of the friction factor behavior in annuli can be made in terms of the pipe diameter ratio, as shown in Fig. 4. Since the Reynolds number is unique for all configurations, the comparison actually involves the respective friction geometry parameters as given by Eqs. (14), (16), and (18). Analyzing the comparison made in Fig. 4, the following can be observed:

- The friction geometry parameter is: constant for circular pipe (pipe diameter ratio equal to zero); a function of the pipe diameter ratio for a concentric annulus; and, a function of both pipe diameter ratio and eccentricity for an eccentric annulus.
- For the concentric annulus, when $k \rightarrow 1$, the friction geometry parameter approaches 24, which is the correct value for flow between infinite parallel plates.
- For a fixed diameter ratio, the friction geometry parameter, and consequently the friction factor, decreases with an increase in the degree of eccentricity.
- For a high degree of eccentricity, the friction geometry parameter, and consequently the friction factor, is always smaller than for a circular pipe.

Finally, the error involved in predicting friction factor values in annulus configurations by applying the hydraulic diameter

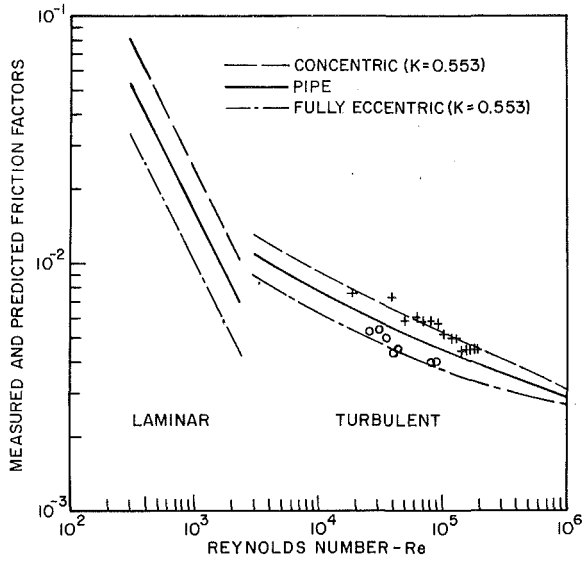

Fig. 5 Fanning friction factor model performance

concept can vary between −40 to 50 percent, depending on the annulus pipe diameter ratio and the degree of eccentricity. This is demonstrated by the dashed line in Fig. 4, which represents the expected friction geometry parameter values for the experimental facility used in this study ($K=0.553$) (Caetano, 1986).

The comparison between friction pressure drop behavior in circular pipes and annuli is now considered. Here it is also assumed that the same fluid and the same flow rate exists in all configurations. Although the hydraulic diameter is the same for all configurations, the area for flow varies, as given by

$$\frac{A_{CA}}{A_P}=\frac{A_{EA}}{A_P}=\frac{(1+K)}{(1-K)} \tag{22}$$

For the same flow rates, the relationship between the average axial velocities is

$$\frac{<V_{CA}>}{<V_P>}=\frac{<V_{EA}>}{<V_P>}=\frac{(1-K)}{(1+K)} \tag{23}$$

Using the relationship given by Eqs. (22) and (23) and the expression given for average axial velocity in circular pipe, a concentric annulus, and an eccentric annulus it can be shown that

$$\frac{[(\pi_o-\pi_L)/L]_{CA}}{[(\pi_o-\pi_L)/L]_P}=\frac{F_{CA}}{F_P}\frac{(1-K)}{(1+K)} \tag{24}$$

and

$$\frac{[(\pi_o-\pi_L)/L]_{EA}}{[(\pi_o-\pi_L)/L]_P}=\frac{F_{EA}}{F_P}\frac{(1-K)}{(1+K)} \tag{25}$$

The left-hand side of these expressions represents the ratio between the friction pressure gradients in an annulus and a circular pipe. Again, large errors can be introduced by applying the hydraulic diameter concept, depending on the pipe diameter ratio and eccentricity.

Turbulent Flow. The Fanning friction factor for an annulus under turbulent single-phase flow, as described in the Literature Survey, can be predicted mainly by three categories of procedures: empirical correlation, semi-empirical correlation, and universal velocity distribution. Comparing these three procedures, in terms of difficulty of application and resulting performance, the following can be concluded: empirical methods should be used only to estimate a value for friction factor; semi-empirical procedures have a desirable combination of a low degree of application difficulty and acceptable performance; finally, a universal velocity distribution type procedure should be used if more than an overall value is sought. Thus, considering the objective of friction factor determination, it was decided to adopt the semi-empirical procedure.

In this study, the Gunn and Darling (1963) approach was chosen to predict turbulent flow friction factor values in annuli, due to its simplicity and good performance. The approach combines the behavior for friction factor in noncircular configurations as given by Eq. (5), with a large amount of turbulent flow data for many noncircular configurations. Combining the Gunn and Darling developments into a Nikuradse-type expression, the friction factor for concentric and eccentric annuli are predicted, respectively, from

$$\frac{1}{\left\{f_{CA}\left(\frac{F_P}{F_{CA}}\right)^{0.45\exp[-(\mathrm{Re}-3000)/10^6]}\right\}^{1/2}}=4.0\log\left\{\mathrm{Re}\left[f_{CA}\left(\frac{F_P}{F_{CA}}\right)^{0.45\exp[-(\mathrm{Re}-3000)/10^6]}\right]^{1/2}\right\}-0.40 \tag{26}$$

and

$$\frac{1}{\left\{f_{EA}\left(\frac{F_P}{F_{EA}}\right)^{0.45\exp[-(\mathrm{Re}-3000)/10^6]}\right\}^{1/2}}=4.0\log\left\{\mathrm{Re}\left[f_{EA}\left(\frac{F_P}{F_{EA}}\right)^{0.45\exp[-(\mathrm{Re}-3000)/10^6]}\right]^{1/2}\right\}-0.40 \tag{27}$$

In these equations, f is the Fanning friction factor and F is the laminar flow friction geometry parameter presented in a previous section.

Comparison With Experimental Data. Data were collected for single-phase turbulent water flow in concentric and fully eccentric annuli, with Reynolds numbers based on Eq. (13) in the range of 10^4 to 2×10^5. The friction pressure drop was measured and Fanning friction factors were calculated for each test using Eq. (12). For the same test conditions, Fanning friction factors are also predicted by the proposed model, using Eqs. (26) or (27).

Comparisons between the calculated and predicted values of Fanning friction factors for concentric and fully eccentric annuli are given in Fig. 5. This figure also shows the predicted values for turbulent friction factor in a pipe with the same hydraulic diameter as for the annuli. Also shown are the predicted friction factor curves for laminar flow through these three different flow configurations.

Figure 5 shows that, for the same hydraulic diameter, there is a considerable difference between friction factor values in an annulus as compared to circular pipe. Usually the friction factor for a concentric annulus is higher than for pipe flow; however, for a fully eccentric annulus the friction factor is lower than for pipe flow. This difference is a constant value for laminar flow, and depends on the annulus pipe diameter ratio and the degree of eccentricity. In turbulent flow, the difference between friction factor values for the configurations decreases as the Reynolds number increases. The annulus friction factors approach values for circular pipe at high Reynolds numbers. Comparison between calculated friction factor values and those predicted by Eqs. (26) or (27) shows good agreement.

Taylor Bubble Rise Velocity

The slug flow pattern is characterized by alternate flow of large bubbles, termed Taylor bubble, followed by liquid slugs. The rise velocity of a Taylor bubble is essential for the prediction of liquid holdup and pressure drop in slug flow. However, most of the studies conducted on bubble rise velocity

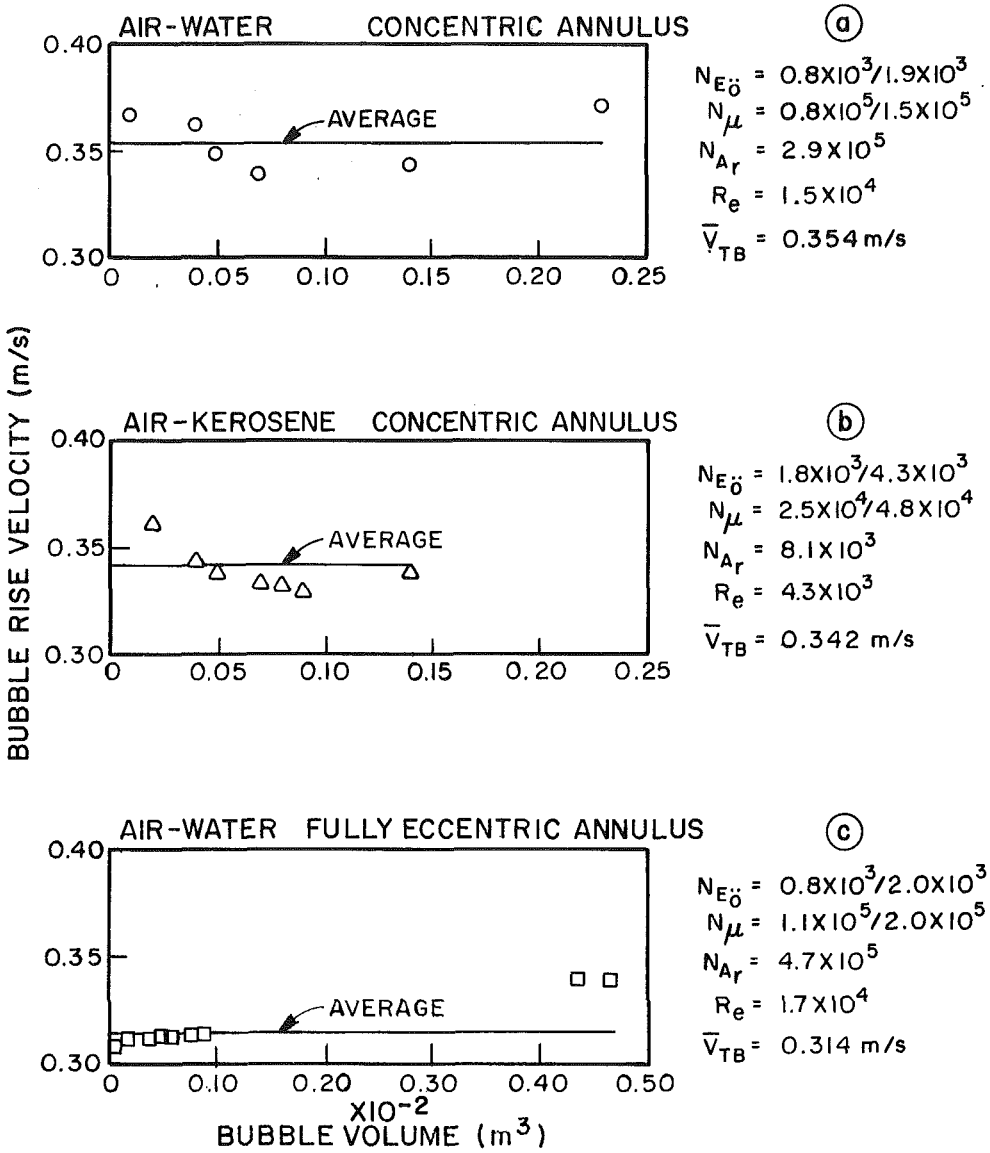

Fig. 6 Experimental Taylor bubble rise velocity in annuli

were for circular pipes and only few studies have involved flow in an annulus.

Taylor bubble rise velocity data acquired in this study are presented in following sections. Also presented is a comparison between the data and existing methods for predicting Taylor bubble rise velocity.

Experimental Taylor Bubble Rise Velocity. Taylor bubble rise velocity data were acquired for air-water and air-kerosene in a concentric annulus, and for air-water in a fully eccentric annulus. The experimental results are reported as a function of the bubble lengths. Figure 6 shows the experimental results. Each point represents various experimental runs having approximately the same bubble length.The straight line drawn for each case represents the overall arithmetic average bubble rise velocity.

Figure 6 also shows the dimensionless number values involved in the bubble rise phenomenon for each case; these include the Eötvos, inverse viscosity and Archimedes numbers as given by Eqs. (6)–(8). In determining these dimensionless groups, two characteristic dimensions were used: the shroud diameter and the equi-periphery diameter given by Eq. (11). The hydraulic diameter was used as the characteristic length for determining Reynolds number. The values obtained for these dimensionless numbers using either characteristic length confirm the inertia dominated nature of the experimental system.

The Taylor bubble in annuli exhibits neither a spherical cap nor a complete symmetry around the axial coordinate, as it normally does in a circular pipe. These deformations are caused by the existence of the axial inner pipe inserted across the bubble. In the fully eccentric annulus, the bubble appears less distorted. In both concentric and eccentric annuli a preferential channel is observed through the rising bubble in which most of the liquid is shed backwards. For any combination of fluid pairs and annuli configurations, the Taylor bubble rise velocity is larger than predicted for a circular pipe with a diameter equal to the annulus shroud diameter. As in the circular pipe case, once the bubble cap is developed, the bubble rise velocity is insensitive to the bubble length and/or volume.

Evaluation of Bubble Rise Velocity Models. The literature survey revealed two empirical models for the prediction of Taylor bubble rise velocity in an annulus, namely the Griffith (1964) model and the Sadatomi et al. (1982) model. A comparison between these models and the experimental data was performed in terms of the dimensionless bubble rise velocity parameter, C_1. However, recall that the concepts used by these investigators were different. .

The Griffith model neglects the bubble density and uses the

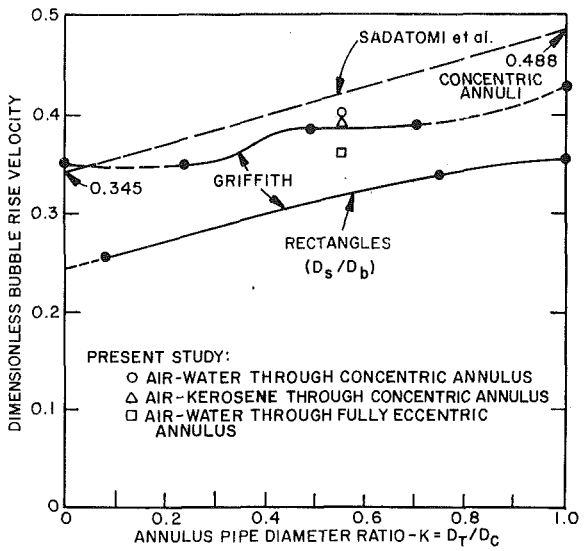

Fig. 7 Comparison of dimensionless Taylor bubble rise velocity parameters

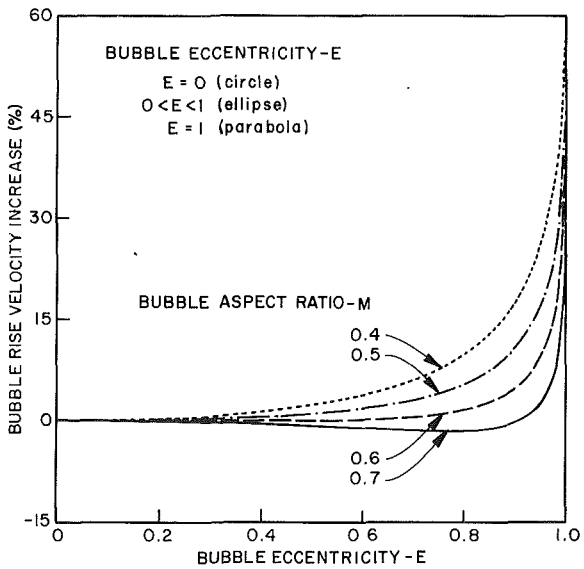

Fig. 8 Theoretical bubble rise velocity increase—Grace and Harrison model

annulus shroud dimension (the inside diameter of the outer pipewall) as the characteristic length. The dimensionless bubble rise velocity parameter, C_1, is given as a function of the annulus pipe diameter ratio, K. Sadatomi et al. used the equi-periphery diameter given by Eq. (11) as the characteristic dimension. Combining Eqs. (10) and (11), the Sadatomi et al. model can be expressed in terms of the annulus shroud dimension

$$V_{TB} = 0.345\sqrt{1+K}\,\sqrt{gD_c} \tag{28}$$

The dimensionless bubble rise velocity parameter is then given by

$$C_1 = 0.345\sqrt{1+K} \tag{29}$$

where K is the annulus pipe diameter ratio and D_C is the annulus shroud diameter.

It is now possible to compare the predictions of the two models. Figure 7 shows the prediction of the two models, along with the three experimental values for the average dimensionless bubble rise velocity determined in this study. Both models reduce to the values predicted for pipe flow as K approaches zero. When K approaches 1, indicating a parallel plate configuration, the two models deviate and the Sadatomi et al. model predicts higher bubble rise velocity values.

Considering only the annulus pipe diameter ratio investigated in this study, the two models seem to set appropriate limiting values for the parameter C_1 for a concentric annulus. The fully eccentric annulus case was not investigated by Griffith or Sadatomi et al. The observed dimensionless bubble rise velocity parameter for the fully eccentric annulus is smaller than that for the concentric annulus and also smaller than predicted by either models. However, this lower velocity for a fully eccentric annulus is still higher than found for a circular pipe with the same shroud diameter. In a fully eccentric annulus, the observed bubbles present a unique cap shape and no longer completely wrap the inner pipe. These aspects are believed to make the eccentric annulus more similar to parallel plates configuration, which would explain the bubble rise velocity for this case.

The theoretical model developed by Grace and Harrison (1967), unfortunately, requires input information which is seldom available before experiments are conducted. However, it can be used to explain and set boundaries for the Taylor bubble rise phenomenon in an annulus. The Grace and Harrison model predicts an increase in the rise velocity for a bubble changing its shape (eccentricity) and aspect ratio for a constant area. In a two-dimensional bubble, the eccentricity, E, varies from zero (circular cap) to one (parabolic cap) and exhibits an elliptical cap for intermediate eccentricity values. The bubble aspect ratio, M, is the ratio between the bubble cap height and the bubble cap width and denotes the degree of bubble flatness or elongation. Figure 8 shows the prediction of this model in terms of percent increase in the bubble rise velocity as a function of E and M. As shown in the figure, a bubble having a change in cap shape from circular to parabolic is expected to have a percent increase in rise velocity of 60, 47, and 35 percent for respective bubble aspect ratio of 0.4, 0.5 and 0.6. The experimental results of Grace and Harrison had an average value of 0.4 for the bubble aspect ratio. The predictions of their model for this value of M agree well with their experimental data. For certain degrees of eccentricity, a bubble with an aspect ratio equal to 0.7 or larger will result in predicting a decrease in velocity. However, this seems to be a limiting value since none of the experimental results reported includes values of M larger than 0.7. For the high values of eccentricity and aspect ratio normally found, the Grace and Harrison model predicts an increase of up to 40 percent in the bubble rise velocity and thus provides theoretical support for the experimental results and models plotted in Fig. 7. A change in shape and nonsymmetry results in higher velocities. Also, an increase in velocity occurs when increasing the inserted area across a Taylor bubble rising in an annulus.

Because of its simplicity and performance, the Sadatomi et al. model was selected in this study to predict Taylor bubble rise velocity in annuli for inertia-dominated phenomenon.

Flow Pattern Transitions

Most of the studies published on flow pattern transitions for upward vertical flow deal with pipe flow configurations. The only studies that dealt with flow pattern transitions in annuli demonstrated a lack of both experimental data and theoretical development.

This section presents flow pattern definitions and experimental flow pattern maps for annuli configurations. The Taitel et al. (1980) model for flow pattern transitions in pipe flow is modified to enable flow pattern prediction in an annulus.

Flow Pattern Definitions. There is a trend to standardize flow pattern classifications and definitions for upward vertical pipe flow (Shoham, 1982). This trend attempts to minimize the number of flow pattern classifications, yet uses acceptable definitions for two-phase flow researchers. Recent published works on flow patterns for upward vertical pipe flow suggest

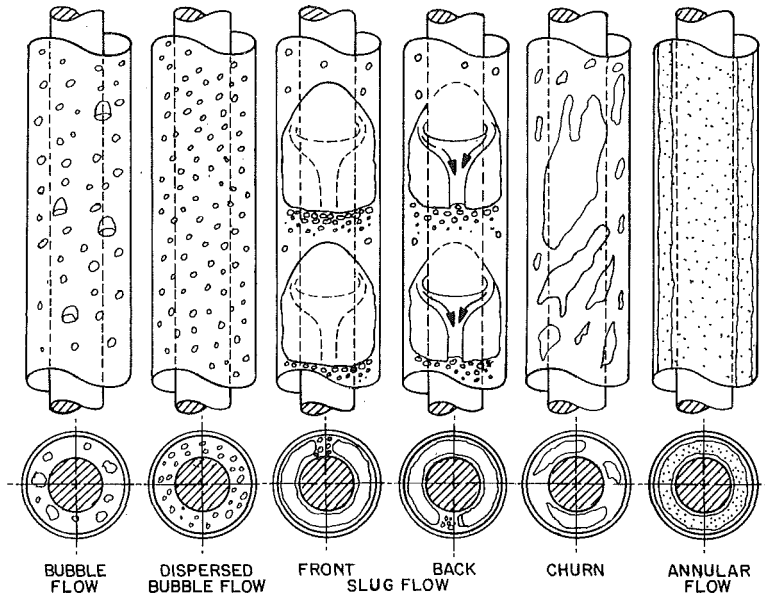

Fig. 9 Flow patterns in upward vertical flow through a concentric annulus

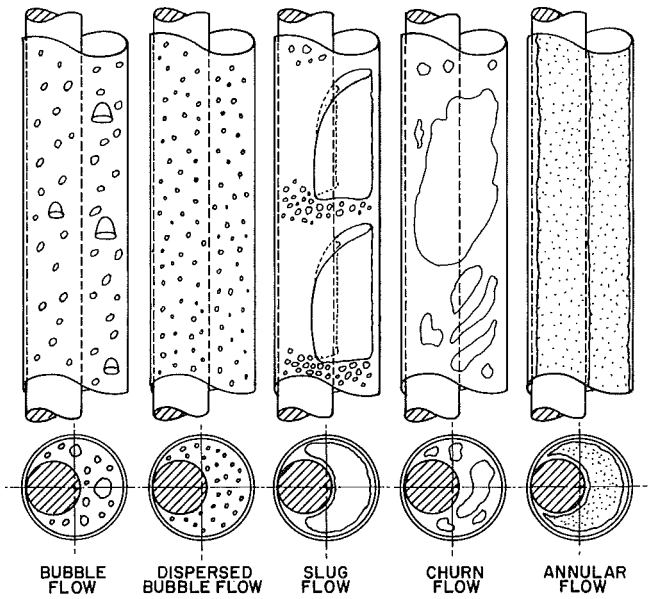

Fig. 10 Flow patterns in upward vertical flow through a fully eccentric annulus

the occurrence of five basic flow patterns: bubble, dispersed bubble, slug, churn, and, annular. The experimental data collected in this study reveal that, although the same flow patterns occur in annuli, their characteristics can be substantially different. Thus, it is essential to define the flow patterns in these configurations.

Figures 9 and 10 show a pictorial view of the flow patterns occurring in concentric and fully eccentric annuli, respectively. Following are the descriptions of these flow patterns.

Bubble Flow (*BB*). The gas phase is dispersed into small discrete bubbles in a continuous liquid phase, forming an approximately homogeneous flow through the annulus cross-sectional area. The discrete bubbles occur in two different shapes, namely spherical bubbles and cap bubbles. The spherical bubbles are very small, on the order of 3–5 mm, as compared to the annulus cap bubbles which are relatively larger, but still always smaller, than half of the configuration hydraulic diameter. The upward movement of the small spherical bubbles follows a zigzag path, whereas the cap bubbles follow a straight path with a faster rise velocity. In a fully eccentric annulus there is a tendency of the small bubbles and the cap bubbles to migrate into the widest gap of the annulus cross-sectional area. This causes a higher local void fraction in this area, relative to the cross-sectional average void fraction.

Dispersed Bubble Flow (*DB*). The gas is distributed as small discrete bubbles within a continuous liquid phase. The spherical shaped bubbles are the only ones observed in this flow pattern. These spherical bubbles are always small and always move straight upward, not showing any zigzag movement. Due to the high liquid velocities encountered in this flow pattern, the mixture appears to flow at the same velocity with no slippage between the phases. This flow pattern is identical in both concentric and fully eccentric annuli configurations.

Slug Flow (*SL*). This flow is characterized by large cap bubbles of gas moving upwards, following by liquid slugs, which bridge the entire cross-sectional area and contain small spherical distributed gas bubbles. The large gas bubbles, which occupy almost the entire cross-sectional area of the annulus, are similar to the ones occurring in pipe flow and are also termed as Taylor bubbles. The Taylor bubbles do not occupy the total cross-sectional area since they have a preferential channel through which most of the liquid ahead of the bubble flows backwards (see Fig. 9). This preferential channel exists from the top to the bottom of the bubble, and from the tubing wall to the casing wall. Due to the presence of this channel, no symmetry is observed for the Taylor bubble with respect to either vertical or horizontal planes. The liquid phase flow backwards in the form of films, around the Taylor bubble, and through the preferential channel, wetting both the tubing and the casing walls. This tends to create a high turbulent region behind the Taylor bubble. Contrary to the concentric annulus case, for a fully eccentric annulus, the preferential liquid channel is always located at the region where the pipe walls are in contact.

Churn Flow (*CH*). This flow is somewhat similar to slug flow. However, it is much more chaotic, frothy and disordered. The Taylor bubble becomes narrow and its shape is destroyed. The continuity of the liquid in the liquid slug between successive Taylor bubbles is also repeatedly destroyed by a high local gas phase concentration. As this happens, the liquid in the slug falls backward, accumulates, forms a temporary bridge and is again lifted upward by the gas. This alternating direction

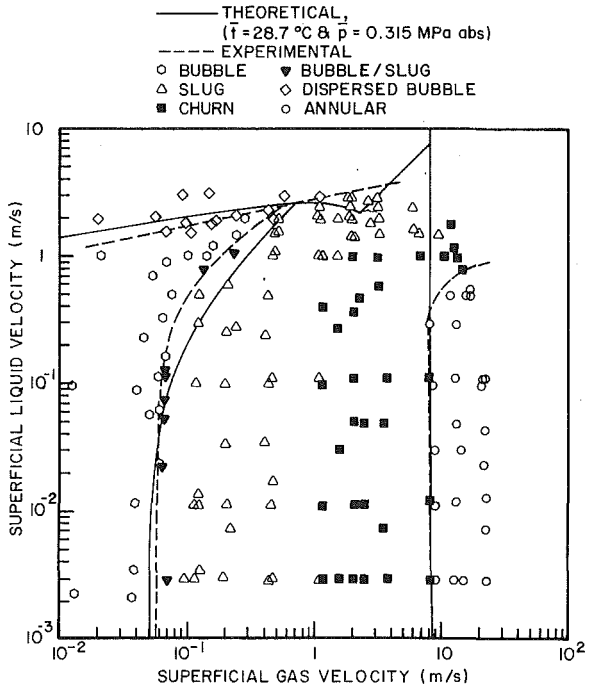

Fig. 11 Flow pattern map for air-water—concentric annulus

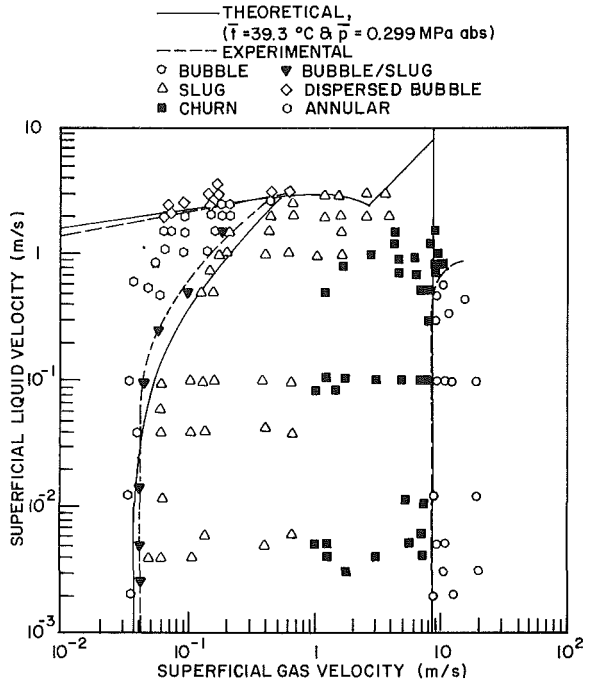

Fig. 13 Flow pattern map for air-water—fully eccentric annulus

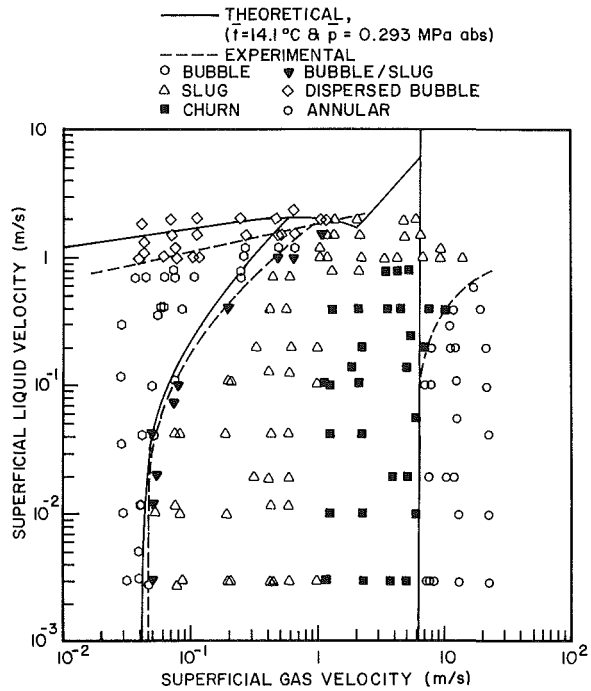

Fig. 12 Flow pattern map for air-kerosene—concentric annulus

for the liquid movement is a typical characteristic of churn flow. This flow pattern is also independent of the annuli configuration.

Annular Flow (AN). The gas is a continuous phase flowing in the core of the annulus cross-sectional area. The liquid flows upward, partially as wavy films around the tubing and casing walls, and partially in the form of tiny spherical droplets entrained in the gas core. The outer film that wets the casing wall is always thicker than the inner film flowing on the tubing wall.

An additional characteristic of annular flow in a fully eccentric annulus is liquid accumulation near the pipe wall contact point. This accumulation results from the merging of the casing and tubing liquid films, which probably happens as a result of the low local gas velocities.

Comparison between flow patterns occurring in upward vertical flow in a pipe and in an annuli reveals that the existence of an inner pipe in the annulus changes the slug and the annular flow patterns. The Taylor bubbles in annuli are not symmetric, having a preferential liquid flow channel through which most of the liquid phase is shed backwards. Two films exist in the annular flow pattern, one flowing around the tubing wall and one around the casing wall. These modifications in flow patterns seem to be a function of the pipe diameter ratio and the eccentricity of the annulus.

Experimental Flow Pattern Maps. Experimental flow pattern data were acquired for air-water and air-kerosene flow through a concentric annulus, and for air-water flow through a fully eccentric annulus. Flow patterns were determined visually, according to the definitions presented previously. The flow pattern data are presented in the form of flow pattern maps, using the gas and liquid superficial velocities as mapping coordinates.

The experimental flow pattern maps obtained for air-water and for air-kerosene flow through the concentric annulus are given in Figs. 11 and 12, respectively. Figure 13 shows the experimental flow pattern map obtained for air-water flow through the fully eccentric annulus. The experimental transition boundary lines between flow pattern regions are given in Figs. 11–13 by dashed lines.

Comparing the experimental flow pattern maps for air-water flow in concentric and fully eccentric annuli, the eccentric annulus has an earlier onset for the bubble to slug flow transition and a later onset for the bubble to dispersed bubble flow transition. However, no major difference was observed for the churn to annular flow transition in these configurations. Comparing the experimental flow pattern maps for air-water flow and air-kerosene flow in the concentric annulus, some fluid property effects can be observed. The air-kerosene mixture presents earlier onset for the bubble to slug flow, bubble to dispersed bubble flow and churn to annular flow transition than found with the air-water mixture.

The experimental characteristics of the flow patterns and flow pattern transitions observed and presented in this section

were used to modify the Taitel et al. (1980) model for flow pattern prediction. The modified model for annuli follows.

Flow Pattern Transition Prediction. The mechanistic model for flow pattern transition prediction in upward vertical two phase flow through circular conduits developed by Taitel et al. is based on the physical mechanisms causing transition between the various flow patterns and incorporates important flow variables such as liquid and gas flow rates, physical properties, and pipe diameter.

Initially, the Taitel et al. model was applied to predict the flow pattern transition boundaries in a concentric annulus. The annulus characteristic dimension was represented by both the hydraulic diameter and its equivalent diameter—a diameter for a pipe which has the same cross-sectional area as the actual annulus. Neither concept when applied to the Taitel et al. flow pattern transition model performed satisfactorily. The main weaknesses were in the prediction of the bubble to slug flow pattern transition at low liquid flow rates, the transition to dispersed bubble flow, and prediction of the existence of the bubble flow region. Hence, modifications of the Taitel et al. flow pattern transition model were necessary to enable flow pattern prediction for an annulus. This work was done by incorporating the experimental observations and the geometric characteristics of the annulus. The modified model as well as its evaluation against the experimental results are presented in the remainder of this section.

Bubble Flow Region Existence. The existence of bubble flow is determined by the different characteristic velocities of the small bubble and the Taylor bubble. The velocity of the discrete bubbles is dependent only on phase physical properties and independent of pipe diameter. However, the Taylor bubble rise velocity, for inertia-dominated conditions, does depend on the pipe diameter. Taitel et al. suggested that whenever the discrete bubble rise velocity is larger than the Taylor bubble rise velocity, the discrete bubbles approach the back of a Taylor bubble and coalescence takes place. When this occurs, bubble flow cannot exist. When the Taylor bubble rises faster than the discrete bubbles, the occasionally occurring Taylor bubble rises through an array of discrete bubbles. Coalescence does not take place as the discrete bubbles are swept around the front of the Taylor bubble. Thus, the Taylor bubble will disappear from the pipe, allowing the existence of the bubble flow pattern.

For a given two-phase fluid pair, there is a limiting value of the configuration characteristic dimension, below which the bubble flow region does not exist. Applying the same mechanisms for determining the existence of the bubble flow region, the following criterion is developed for the annulus.

The discrete bubble rise velocity, after Harmathy (1955), is given by

$$V_{0,\infty} = 1.53\left[\frac{(\rho_L-\rho_G)g\sigma}{\rho_L^2}\right]^{1/4} \tag{30}$$

which depends only on the physical properties of the phases.

The Taylor bubble rise velocity for inertia-dominated conditions in an annulus can be predicted by

$$V_{TB} = 0.345\sqrt{g\ D_{EP}} \tag{10}$$

where D_{EP} is the equi-periphery diameter given by Eq. (11).

Bubble flow can exist if $V_{TB} > V_{0,\infty}$. Hence, combining Eqs. (30) and (10), the bubble flow pattern region in annuli exists when

$$D_{EP} \geq 19.7\sqrt{\frac{(\rho_L-\rho_G)\sigma}{g\ \rho_L^2}} \tag{31}$$

Bubble to Slug Flow Transition. At low superficial liquid velocities, turbulence is negligible and the bubble to slug flow pattern transition is controlled by an agglomeration mechanism. When gas is introduced at low flow rates, the gas phase is distributed into discrete bubbles. These bubbles move upward in a zigzag path with considerable randomness, occasionally colliding, coalescing and forming large bubbles. As the gas rate is increased, the bubble size and number increase. A point is reached where the bubbles become closely packed, causing an increase in rate of collision, increasing the rate of agglomeration, and finally causing a transition to the slug flow pattern. Taitel et al. suggested that for uniformly distributed bubbles, the transition occurs when the gas void fraction reaches 0.25.

For flow through the concentric annulus, an average gas void fraction value of 0.20 was measured at the bubble to slug transition boundary. This lower value is due to the pressure of cap bubbles, probably because of the small gap dimension.

For flow through the fully eccentric annulus, a still lower gas void fraction value of 0.15 was measured at the bubble to slug transition boundary. Besides the bubble shape aspect effects mentioned in the concentric case, here a migration of the bubbles to the widest gap region is also observed. Hence, this region with local high gas void fraction can cause the bubble to slug flow transition to occur at lower average void fraction. Studying upward vertical gas-liquid flow through a rod bundle configuration, Venkateswararao et al. (1982) also observed a migration of the bubbles to a wider region among the rods. Similarly, lower values for the gas void fraction at the bubble to slug flow transition were experimentally determined.

Thus, the Taitel et al. model is modified for the bubble to slug transition in an annulus by using values of the gas void fraction measured at this transition. The resulting equation for the transition can now be developed.

The in-situ gas and liquid velocities are related by

$$\frac{V_{SG}}{H_G} = \frac{V_{SL}}{H_L} + V_{0,\infty} \tag{32}$$

where $V_{0,\infty}$ is the discrete bubble rise velocity given by Eq. (30).

Substituting Eq. (30) in Eq. (32) and using the measured values for the gas void fraction at the bubble to slug flow pattern transition, i.e., 0.2 and 0.15 for concentric and fully eccentric annuli, respectively, yields

$$V_{SG} = \frac{V_{SL}}{4.0} + 0.306\left[\frac{(\rho_L-\rho_G)g\sigma}{\rho_L^2}\right]^{1/4} \tag{33}$$

and

$$V_{SG} = \frac{V_{SL}}{5.67} + 0.230\left[\frac{(\rho_L-\rho_G)g\sigma}{\rho_L^2}\right]^{1/4} \tag{34}$$

Equations (33) and (34) constitute the criteria for the bubble to slug transition boundary at low liquid flow rates, in the concentric and fully eccentric annuli, respectively.

Bubble or Slug to Dispersed Bubble Flow Transition. At high superficial liquid velocities, Taitel et al. suggested that turbulent forces causes the gas phase in either slug or bubble flow patterns to break into small bubbles and become dispersed in the continuous liquid phase. When the turbulent fluctuation intensity is sufficiently high to break the Taylor bubbles into fine bubbles, smaller than a critical bubble size to prevent reagglomeration, then dispersed bubble flow will occur. Using the hydraulic diameter concept, the expression for the bubble or slug to dispersed bubble flow transition becomes

$$2\left[\frac{0.4\sigma}{(\rho_L-\rho_G)g}\right]^{1/2}\left(\frac{\rho_L}{\sigma}\right)^{3/5}\left(\frac{2}{D_H}\right)^{2/5}(f)^{2/5}(V_M)^{6/5} = 0.725 + 4.15\left(\frac{V_{SG}}{V_M}\right)^{1/2} \tag{35}$$

V_M is the mixture superficial velocity and f is the Fanning friction factor evaluated for the homogeneous mixture flowing

in either the concentric or eccentric annulus, as given by Eqs. (26) and (27), respectively.

For a uniform bubble size distribution and a cubic lattice packing, the maximum allowable gas void fraction under dispersed bubble conditions is 0.52. Higher values of void fraction will cause transition to slug flow. Using this criterion and Eqs. (30) and (32) yields the following transition boundary to dispersed bubble flow for gas void fractions above 0.52:

$$V_{SG} = 1.083\ V_{SL} + 0.796\left[\frac{(\rho_L - \rho_G)g\sigma}{\rho_L^2}\right]^{1/4} \quad (36)$$

Transition to Annular Flow. For pipe flow, Taitel et al. suggested that the mechanism causing transition to annular flow is related to the minimum gas velocity necessary to transport upward the largest liquid droplet entrained in the gas core. For lower gas velocities, the liquid droplets would fall back, accumulate, form a bridge and churn or slug flow would prevail.

The required minimum gas velocity is determined from a balance between gravity and drag forces acting on the largest stable droplet. Neglecting the effect of the film thickness, the transition is given by

$$V_{SG} \geq 3.1\left[\frac{(\rho_L - \rho_G)g\sigma}{\rho_L^2}\right]^{1/4} \quad (37)$$

Evaluation of Flow Pattern Transition Model. The modified model was tested against the experimental data acquired for each pair of fluids in the respective annulus. The solid lines in Figs. 11, 12, and 13 constitute the transition boundaries predicted by the modified model. These predictions were made for the average experimental values for temperature and pressure shown in the maps. With the exception of the annular transition at high liquid flow rates, excellent agreement exists between the experimentally obtained boundaries (broken lines) and the theoretically predicted boundaries (solid lines).

Conclusions

An experimental annulus system was designed and constructed. The system can operate under both concentric and fully eccentric configuration.

The experimental data included single-phase friction factor, Taylor bubble rise velocity and two-phase flow maps.

Analysis of single-phase flow friction factors revealed the inadequacy of the hydraulic diameter application for flow conditions at low Reynolds numbers. The analysis showed that for flow through an annulus, the friction factor depends on the Reynolds number, configuration pipe diameter ratio and degree of eccentricity. A semi-empirical model was developed for turbulent which incorporates the analytical results obtained under laminar flow conditions.

The Taylor bubble rise velocity in an annulus increases in comparison to full pipe flow. This is due to the insertion of the tubing through the bubble, which results in a change of bubble cap shape. Also, the bubble rise velocity increases with a decrease of the hydraulic diameter. The Sadatomi et al. (1968) model was found to predict the bubble rise velocity adequately.

The model developed by Taitel et al. (1980) for flow pattern prediction in upward vertical pipe flow was modified to predict flow patterns in annuli. In general, good agreement exist between the experimental data and the predicted results.

Acknowledgments

The authors wish to thank the Tulsa University Fluid Flow Projects (TUFFP) member companies supporting this project. This paper was presented at the 4th International Conference on Multi-Phase Flow, organized by BHRA, in Nice, France, June 19–21, 1989. Copies of conference papers can be purchased from BHR Group.

References

Bird, R., Stewart, W., and Lightfoot, E., 1976, *Transport Pheonomena*, John Wiley and Sons.

Caetano, F. E., 1985, "Upward Vertical Two-Phase Flow Through an Annulus," Ph.D. dissertation, The University of Tulsa.

Davis, R. M., and Taylor, G. I., 1950, "The Mechanism of Large Bubbles Rising Through Liquids in Tubes," *Proceedings of the Royal Society*, Vol. 200, Ser. A., pp. 375–390.

Deissler, R. G., and Taylor, M. F., 1955, "Analysis of Fully Developed Turbulent Heat Transfer and Flow in an Annulus with Various Eccentricities," NACA TN-3451.

Dodge, N. A., 1964, "Friction Losses in Annular Flow," ASME PN 63-WA-11.

El-Saden, M. R., 1961, "Heat Conduction in an Eccentrically Hollow, Infinitely Long Cylinder with Internal Heat Generation," ASME *Journal of Heat Transfer*, Vol. 83, pp. 510–513.

Govier, G. W., and Aziz, K., 1977, *The Flow of Complex Mixtures in Pipes*, Krieger.

Grace, J. R., and Harrison, D., 1967, "The Influence of Bubble Shape on the Rising Velocities of Large Bubbles," *Chemical Engineering Science*, Vol. 22, pp. 1337–1347.

Griffith, P., 1964, "The Prediction of Low-Quality Boiling Voids," *Journal of Heat Transfer*, Aug., pp. 327–333.

Gunn, D. J., and Darling, C. W. W., 1963, "Fluid Flow and Energy Losses in Non-Circular Conduits," *Transactions of the Institution of Chemical Engineers*, Vol. 41, pp. 163–173.

Harmathy, T. Z., 1955, "Velocity of Large Drops and Bubbles in Media of Infinite or Restricted Extent," *AIChE Journal*, Vol. 1, p. 289.

Hinze, J. O., 1959, *Turbulence*, McGraw-Hill.

Jonsson, V. K., and Sparrow, E. M., 1966, "Experiments on Turbulent-Flow Phenomena in Eccentric Annular Ducts," *Journal of Fluid Mechanics*, Vol. 25, pp. 65–86.

Knudsen, J. G., and Katz, D. L., 1954, *Fluid Dynamics and Heat Transfer*, Engineering Research Institute, University of Michigan.

Lawn, C. J., and Elliott, C. J., 1972, "Fully Developed Turbulent Flow Through Concentric Annuli," *Journal of Mechanical Engineering and Science*, Vol. 14, pp. 195–204.

Mukherjee, H., 1979, "An Experimental Study of Inclined Two-Phase Flow," Ph.D. dissertation, The University of Tulsa.

Quarmby, A., 1967, "An Experimental Study of Turbulent Flow Through Concentric Annuli," *International Journal of Mechanical Science*, Vol. 9, pp. 205–221.

Redberger, P. J., and Charles, M. E., 1962, "Axial Laminar Flow in a Circular Pipe Containing a Fixed Eccentric Core," *Canadian Journal of Chemical Engineering*, pp. 148–151.

Rothfus, R. R., and Newby, R. A., 1970, "Transactional Flow in Concentric Annuli," *AIChE Journal*, Mar., Vol. 16, pp. 173–177.

Rothfus, R. R., Sartory, W. K., and Kermode, R. I., 1966, "Flow in a Concentric Annuli at High Reynolds Numbers," *AIChE Journal*, Nov., Vol. 12, pp. 1086–1091.

Rothfus, R. R., Walker, J. E., and Whan, G. A., 1958, "Correlation of Local Velocities in Tubes, Annuli, and Parallel Plates," *AIChE Journal*, June, Vol. 4, pp. 240–245.

Sadatomi, M., Sato, Y., and Saruwatari, S., 1982, "Two-Phase Flow in Vertical Noncircular Channels," *International of Journal of Multiphase Flow*, Vol. 8, pp. 641–655.

Salcudean, M., Chun, J. H., and Groeneveld, D. C., 1983, "Effect of Flow Obstructions on Void Distribution in Horizontal Air-Water Flow," *International Journal of Multiphase Flow*, Vol. 9, pp. 91–96.

Salcudean, M., Chun, J. H., and Groeneveld, D. C., 1983, "Effect of Flow Obstructions on the Flow Pattern Transitions in Horizontal Two-Phase Flow," *International Journal of Multiphase Flow*, Vol. 9, pp. 87–90.

Salcudean, M., Groeneveld, D. C., and Leung, L., 1983, "Effect of Flow-Obstruction Geometry on Pressure Drops in Horizontal Air-Water Flow," *International Journal of Multiphase Flow*, Vol. 9, pp. 73–85.

Shoham, O., 1982, "Flow Pattern Transition and Characterization in Gas-Liquid Two Phase Flow in Inclined Pipes," Ph.D. dissertation, Tel-Aviv University.

Snyder, W. A., and Goldstein, G. A., 1965, "An Analysis of Fully Developed Laminar Flow in an Eccentric Annulus," *AIChE Journal*, Vol. 11, pp. 462–467.

Taitel, Y., Barnea, D., and Dukler, A. E., 1980, "Modelling Flow Pattern Transitions for Steady Upward Gas-Liquid Flow in Vertical Tubes," *AIChE Journal*, Vol. 26, pp. 345–354.

Tosun, I., 1984, "Axial Laminar Flow in an Eccentric Annulus: An Approximate Solution," *AIChE Journal*, Vol. 30, pp. 877–878.

Venkateswararao, P., Semiat, R., and Dukler, A. E., 1982, "Flow Pattern Transition for Gas-Liquid Flow in a Vertical Rod Bundle," *International Journal of Multiphase Flow*, Vol. 8, pp. 509–524.

Wallis, G. B., 1969, *One-Dimensional Two-Phase Flow*, McGraw-Hill.

Winkler, H. W., 1968, "Single and Two-Phase Vertical Flow Through 0.996×0.625 inch Fully Eccentric Plain Annular Configuration," Ph.D. dissertation, The University of Texas at Austin.